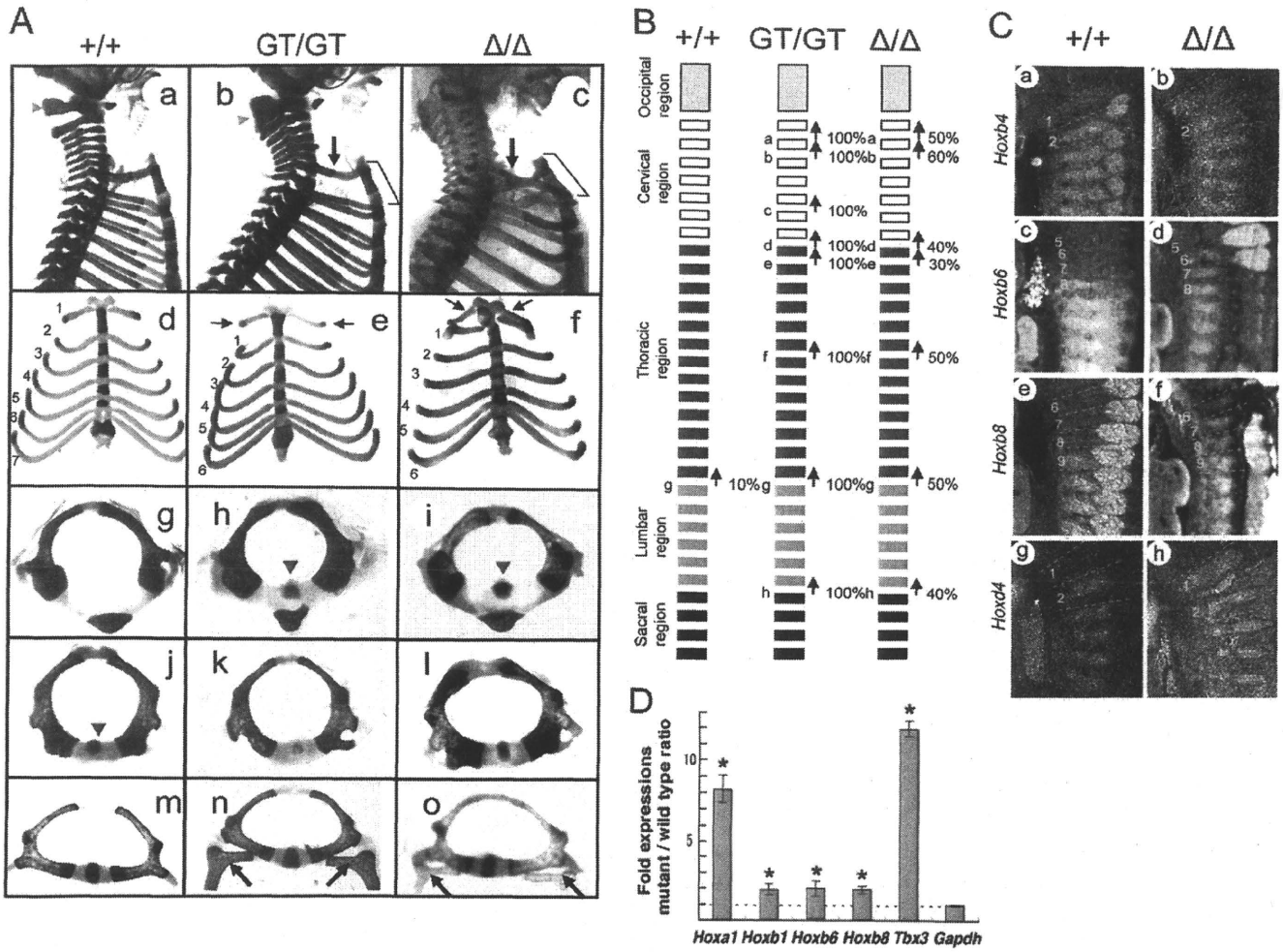

FIG. 2. Posterior transformation of the axis in $Pcl2^{GT/GT}$ and $Pcl2^{\Delta/\Delta}$ mutants. (A) Skeletal alterations in $Pcl2^{GT/GT}$ (GT/GT) and $Pcl2^{\Delta/\Delta}$ (Δ/Δ) mutants. (Frames a, b, and c) Lateral views of the upper part of the vertebral column are shown. Yellow arrowheads indicate the first cervical vertebra. The arrows and brackets in frames b and c indicate the ectopic ribs associated with C7 and the anteriorly shifted sternum, respectively. (Frames d, e, and f) Ventral views of the rib cages are shown. In frames e and f, the ectopic ribs associated with C7 are indicated by arrows. (Frames g, h, and i) Overviews of isolated C1 vertebrae. Odontoid processes fused with C1 are indicated by arrowheads in frames h and i. (Frames j, k, and l) Overviews of isolated C2 vertebrae. The odontoid process is indicated by an arrowhead in frame j. (Frames m, n, and o) Overviews of isolated C7 vertebrae. Ectopic ribs are indicated by arrows in frames n and o. (B) Schematic summary of the axial homeotic transformations in $Pcl2^{GT/GT}$ and $Pcl2^{\Delta/\Delta}$ mice. The following parameters, identified by letters on the figure, were scored, and the frequency of each alteration is indicated: C1 → C2, presence of the odontoid process on the C1 vertebra (a); C2 → C3, lack of the odontoid process from the C2 vertebra (b); C5 → C6, appearance of anterior tuberculum (c); C7 → T1, appearance of cervical ribs on C7 (d); T1 → T2, prominent spinous process on T1 (e); T7 → T8, dissociation of seventh rib from the sternum (f); T13 → L1, loss of the rib on 20th vertebra (g); lumbar vertebra 5 (L5) or L6 → sacral vertebra 1 (S1), formation of the sacroiliac joint in 25th or 26th vertebra (h). (C) Expression of *Hox* genes in 11.5-dpc wild-type and $Pcl2^{\Delta/\Delta}$ embryos. The expression of *Hoxb4* (a and b), *Hoxb6* (c and d), *Hoxb8* (e and f), and *Hoxd4* (g and h) is shown. Prevertebrae are numbered starting from the proatlas, and dotted lines indicate the segment boundaries. (D) Derepression of *Hox* genes in $Pcl2^{\Delta/\Delta}$ ES cells. *Hoxa1*, *Hoxb4*, *Hoxb6*, *Hoxb8*, and *Tbx3* were derepressed in $Pcl2^{\Delta/\Delta}$ ES cells compared to the wild-type controls by real-time PCR. Fold expression of respective genes in $Pcl2^{\Delta/\Delta}$ ES cells compared to that of the wild type is shown by bars. Statistically significant differences are indicated by asterisks.

A prominent spinous process, which appeared on thoracic vertebra 2 (T2) in the wild-type, $Suz12^{+/-}$, and $Pcl2^{\Delta/\Delta}$ pups, was frequently associated with the T1 in $Pcl2^{\Delta/\Delta}$; $Suz12^{+/-}$ mutants. In summary, heterozygous loss of *Suz12* synergistically enhanced the homeotic transformations of *Pcl2* single mutants. Taken together, we conclude that *Hox* repression by Pcl2 involves its interaction with PRC2. Since Pcl and PHF1 are known to enhance the catalytic activity of PRC2, we inferred that Pcl2 contributes to *Hox* repression by regulating PRC2 activity. We did not, however, observe extensive changes in global and local levels of H3K27me3 in $Pcl2^{\Delta/\Delta}$ ES cells (Fig. 4C and D). Supporting this observation, binding of Ring1B to *Hox* genes was not changed despite *Hox* derepression in ES cells. As the molecular mechanisms that underlie Pcl2-dependent regulation of PRC2 are still unclear, we speculated that Pcl2-mediated *Hox* repression might involve PRC1.

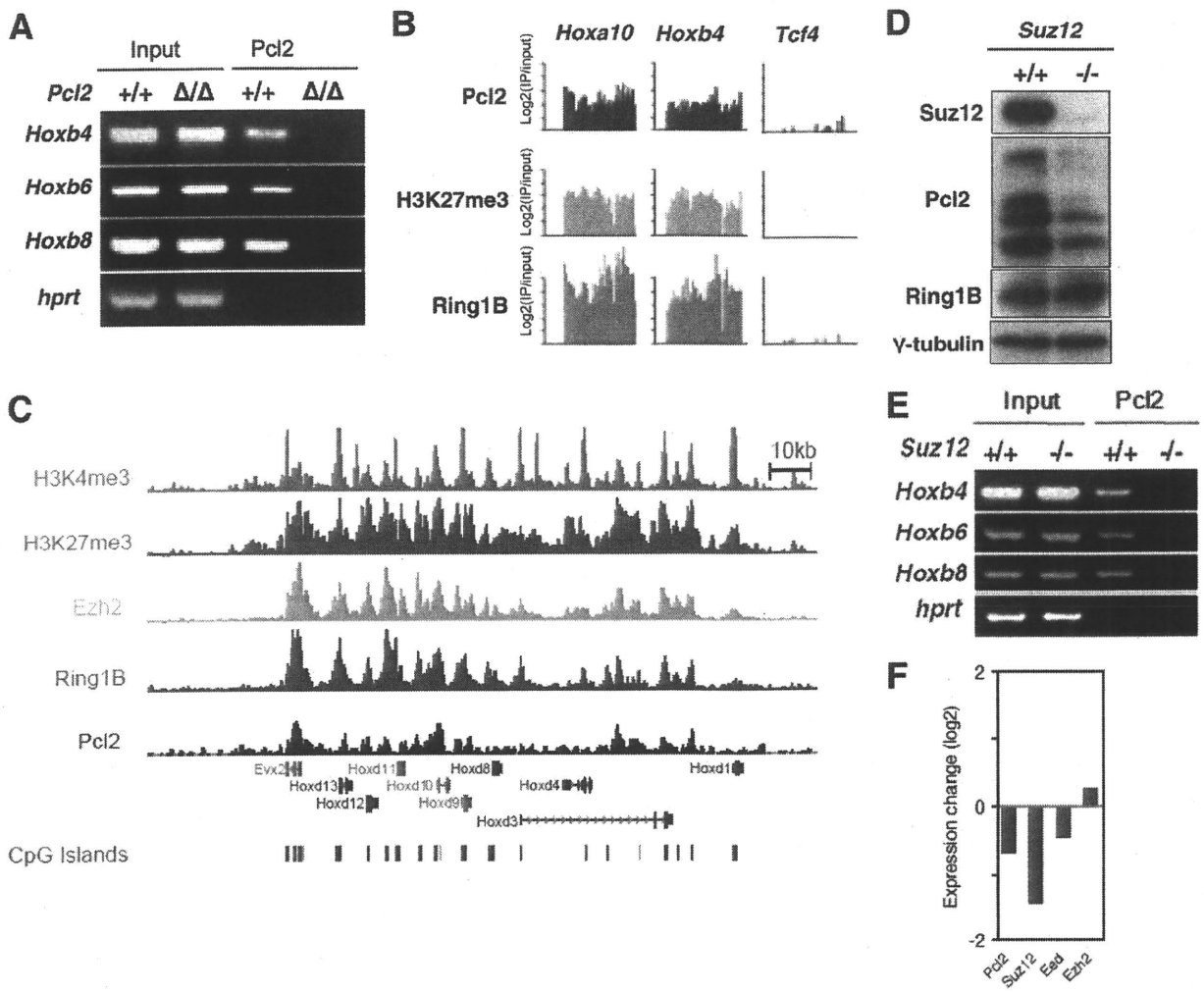

FIG. 3. PRC2-dependent binding of Pcl2 to *Hox* genes. (A) Pcl2 association at *Hox* promoter regions revealed by conventional ChIP assay using anti-N polyclonal in $Pcl2^{+/+}$ (+/+) and $Pcl2^{\Delta/\Delta}$ (Δ/Δ) ES cells. For the input, genomic DNA extracted from the original whole-cell lysate equivalent to 1/40 of the volume used for the ChIP analysis was subjected to PCR; the *hprt* gene was used as a negative control. (B) The distribution of Pcl2, H3K27me3, and Ring1B at the promoter regions of the genes in ES cells. Agilent mouse promoter ChIP-on-Chip Sets 244K were used for *Hoxa10*, *Hoxb4*, and *Tcf4* promoter region analysis. (C) ChIP-seq binding patterns for *Evx2* and *Hoxd* loci are shown for H3K4me3, H3K27me3, Ezh2, Ring1B, and Pcl2 in ES cells. CpG islands are shown as green bars (below). (D) Impact of Suz12 deficiency on the expression of Pcl2. The expression of Suz12, Pcl2, Rnf2, and γ-tubulin in $Suz12^{+/+}$ (+/+) and $Suz12^{-/-}$ (−/−) ES cells as revealed by Western blotting. (E) Pcl2 association at *Hox* promoter regions in $Suz12^{+/+}$ and $Suz12^{-/-}$ ES cells. For the input, genomic DNA extracted from the original whole-cell lysate equivalent to 1/40 of the volume used for the ChIP analysis was subjected to PCR; the *hprt* gene was used as a negative control. (F) Expression changes of *Pcl2*, *Suz12*, *Eed*, and *Ezh2* in $Suz12^{-/-}$ ES cells. Expression changes of *Pcl2*, *Suz12*, *Eed*, and *Ezh2* in $Suz12^{-/-}$ ES cells were revealed by microarray analysis using Affymetrix Mouse 430.2. Detected signals were normalized using a quantile normalization method, and only signals having significant intensity from background were counted. The average signal intensity of respective genes in $Suz12^{-/-}$ and wild-type ES cells was calculated, and the log ratios of $Suz12^{-/-}$ against wild type are shown by bars.

We thus examined whether the *Pcl2* mutation functionally interacts with mutations in genes encoding PRC1 components since previous reports have shown that compound mutants of PRC1 genes have a more severe phenotype than single mutants, suggesting the importance of such cooperativity (2, 6). We therefore compared the axial skeletal abnormalities in $Pcl2^{\Delta/\Delta}$; $Mel18^{-/-}$ and $Pcl2^{\Delta/\Delta}$; $Mel18^{+/+}$ mice. Notably, no viable $Pcl2^{\Delta/\Delta}$; $Mel18^{-/-}$ mice were seen at the perinatal stage, whereas the respective single homozygotes ($Pcl2^{\Delta/\Delta}$; $Mel18^{+/+}$ and $Pcl2^{+/+}$; $Mel18^{-/-}$) survived. Because of this, the skeletal phenotypes were examined at 16.5 dpc. $Mel18^{-/-}$ fetuses had phenotypes that were nearly identical to those in the $Pcl2^{\Delta/\Delta}$ fetuses, as reported previously (1). The $Pcl2^{\Delta/\Delta}$; $Mel18^{-/-}$ double mutants showed more stringent transformations than either of the single mutants (Fig. 5C and D). Occipital bones were segmented, resulting in the formation of an ectopic arch. The C1 vertebrae were identical to the wild-type C2, and perfect ribs bridged an anteriorly shifted sternum and the C7. Interestingly, a hole reproducibly appeared at the central region of the scapula of $Pcl2^{\Delta/\Delta}$; $Mel18^{-/-}$ mice, which was not seen in either of the single mutants. A similar synthetic defect in the scapula has been reported in $Mel18^{-/-}$; $Phc2^{-/-}$ and $Mel18^{-/-}$; $Bmi1^{+/-}$ mice due to the combined effects of the respective mutations (2, 28). Taken together, the genetic in-

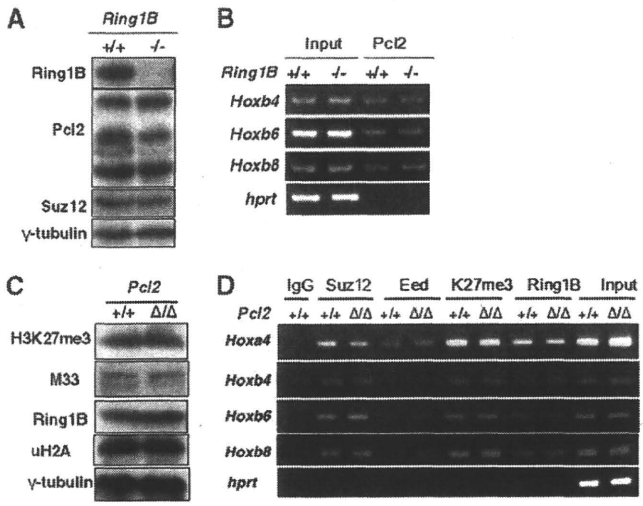

FIG. 4. The expression and target binding of Ring1B and Pcl2 are regulated in a mutually independent manner in ES cells. (A) Pcl2 and Suz12 are expressed in a Ring1B-independent manner. The expression of Ring1B, Pcl2, and Suz12 in *Ring1B*$^{+/+}$ and *Ring1B*$^{-/-}$ ES cells is shown. γ-Tubulin was used as a dose control. (B) Pcl2 binds to *Hox* promoters in a Ring1B-independent manner. Pcl2 association to the *Hox* promoter regions in *Ring1B*$^{+/+}$ and *Ring1B*$^{-/-}$ ES cells is shown. The *hprt* gene was used as a negative control. (C) Global levels of H3K27 trimethylation (H3K27me3), M33, Ring1B, and H2A monoubiquitinylation (uH2A) were not significantly altered in *Pcl2*$^{\Delta/\Delta}$ ES cells (Δ/Δ) compared to levels in the wild type (+/+). γ-Tubulin was used as a dose control. (D) Binding of Suz12, Eed, H3K27me3, and Ring1B at *Hox* promoter regions was not significantly changed in *Pcl2*$^{\Delta/\Delta}$ ES cells (Δ/Δ). IgG and *hprt* genes were used as negative controls.

teractions between *Pcl2* and *Mel18* mutations synergistically enhanced skeletal abnormalities of the respective mutants and influenced the survival of late-gestation fetuses. To further clarify whether interactions between *Pcl2* and *Mel18* involve PRC1, we extended our genetic studies to Phc2, which is another PRC1 component and is known to physically and genetically interact with Mel18 (28). The *Pcl2*$^{\Delta/\Delta}$; *Phc2*$^{-/-}$ fetuses exhibited skeletal phenotypes and late-gestational lethality very similar to the patterns seen in not only *Pcl2*$^{\Delta/\Delta}$; *Mel18*$^{-/-}$ but also *Mel18*$^{-/-}$; *Phc2*$^{-/-}$ and *Phc1*$^{+/-}$; *Phc2*$^{-/-}$ mutants (Fig. 5C and D). These observations indicate a role for Pcl2 in reinforcing *Hox* repression that is mediated by PRC1. The cooccupancy of *Hox* genes by Pcl2 together with PRC2 and PRC1 suggests that Pcl2 positively regulates PRC2 and PRC1 to repress *Hox* genes during A-P specification of the axis.

***Cdkn2a* activation by Pcl2 in MEFs involves suppression of PRC2.** We went on to examine the functional implication of Pcl2 to mediate Polycomb repression in other cellular contexts. Senescence is a fundamental cellular program that is activated under various forms of stress and acts to prevent further cell proliferation. When a population of cells is propagated in culture, they are exposed to various extrinsic and intrinsic stresses, and the cell population gradually stops dividing. Two definitive tumor suppressor pathways, ARF/MDM2/p53 and p16^{INK4a}/Rb, have been shown to play critical roles in the induction of cellular senescence (59). Central mediators for cellular senescence, p19^{arf} and p16^{Ink4a}, are encoded by the *Cdkn2a* locus, which is known as an essential target of PRC1 (30). PRC1 represses p19^{arf} and p16^{Ink4a} in embryonic fibroblasts (MEFs) and thus protects MEFs to some extent from stress-induced premature senescence. This PRC1-dependent regulation of *Cdkn2a* has also been shown to be active in various stem and progenitor cells.

We first examined the binding of Pcl2 to the *Cdkn2a* locus by ChIP-seq analysis and found considerable Pcl2 deposition together with Ezh2, H3K27me3, and Ring1B in ES cells (Fig. 6A). To test the role of Pcl2 in the regulation of p19^{arf} and p16^{Ink4a} expression, we generated MEFs from *Pcl2*$^{\Delta/\Delta}$ and wild-type littermates and compared progression of cellular senescence by a 3T9 assay (Fig. 6B). To our surprise, growth of *Pcl2*$^{\Delta/\Delta}$ MEFs was similar to that of wild-type MEFs until passage 10, but then the cells failed to stop dividing and continued exponential growth over 50 passages while *Phc2*$^{-/-}$ MEFs prematurely senesced. We further found that *Pcl2*$^{GT/GT}$ MEFs similarly bypassed senescence (Fig. 6C). To confirm that this effect is directly due to Pcl2 loss, we expressed Pcl2 in immortalized *Pcl2*$^{GT/GT}$ MEFs by retroviral transduction. Ectopic expression of Pcl2 indeed induced cellular senescence in immortalized *Pcl2*$^{GT/GT}$ MEFs (Fig. 6D). Consistent with these phenotypes, *Pcl2*$^{\Delta/\Delta}$ MEFs did not exhibit morphological features characteristic of senescent MEFs at passage 12 (Fig. 6E). We went on to investigate the expression of p19^{arf} and p16^{Ink4a} in *Pcl2*$^{\Delta/\Delta}$ MEFs and observed their strong repression at passage 10 (Fig. 6F). This was accompanied by a reduction of *p19*^{arf} and *p16*^{Ink4a} transcripts (Fig. 6G). Therefore, these results suggest that *Pcl2*$^{\Delta/\Delta}$ MEFs fail to undergo cellular senescence.

We next tested the functional involvement of *Cdkn2a* repression in terminating cellular senescence. To this end, we expressed p19^{arf} or p16^{Ink4a} in *Pcl2*$^{\Delta/\Delta}$ MEFs by retroviral transduction. Proliferation of *Pcl2*$^{\Delta/\Delta}$ MEFs was clearly inhibited by either p19^{arf} or p16^{Ink4a} (Fig. 6H), thus suggesting that Pcl2 promotes cellular senescence by activating the expression of *Cdkn2a* genes in MEFs. To further test this hypothesis, we overexpressed Pcl2 in MEFs. We generated a transgenic mouse, in which expression of the 67-kDa isoform of Pcl2 could be induced by tamoxifen-dependent activation of ERT2-Cre (Fig. 7A). Proliferation of these MEFs was impaired by tamoxifen treatment (Fig. 7B), and the mitotic arrest was accompanied by activation of p19^{arf} (Fig. 7C). Therefore, we showed that Pcl2 plays a role as an activator of *Cdkn2a* expression, whereas PRC1 functions as a repressor in MEFs.

We went on to test whether this positive effect of Pcl2 on *Cdkn2a* transcription involved regulation of the catalytic activity of PRC2. We performed ChIP analysis to test H3K27me3 occupancy at the *p16*^{Ink4a} promoter region in *Pcl2*$^{GT/GT}$ MEFs (Fig. 8A and B). Local H3K27me3 levels at this promoter were significantly increased in *Pcl2*$^{GT/GT}$ MEFs compared to levels the wild-type cells. Consistent with the transcriptional status of *p16*^{Ink4a}, we also found decrease H3K4me3 in *Pcl2*$^{GT/GT}$ MEFs. Pcl2 therefore activates *Cdkn2a* expression, presumably by suppressing local catalytic activity of PRC2.

In addition, we examined whether Pcl2-dependent regulation of *Cdkn2a* involves PRC1. We generated *Pcl2* and *Phc2* double mutant MEFs and compared the level of cellular senescence to that observed in the single mutants (Fig. 6B). Notably, *Pcl2*$^{\Delta/\Delta}$; *Phc2*$^{-/-}$ MEFs, as well as *Phc2*$^{-/-}$ MEFs,

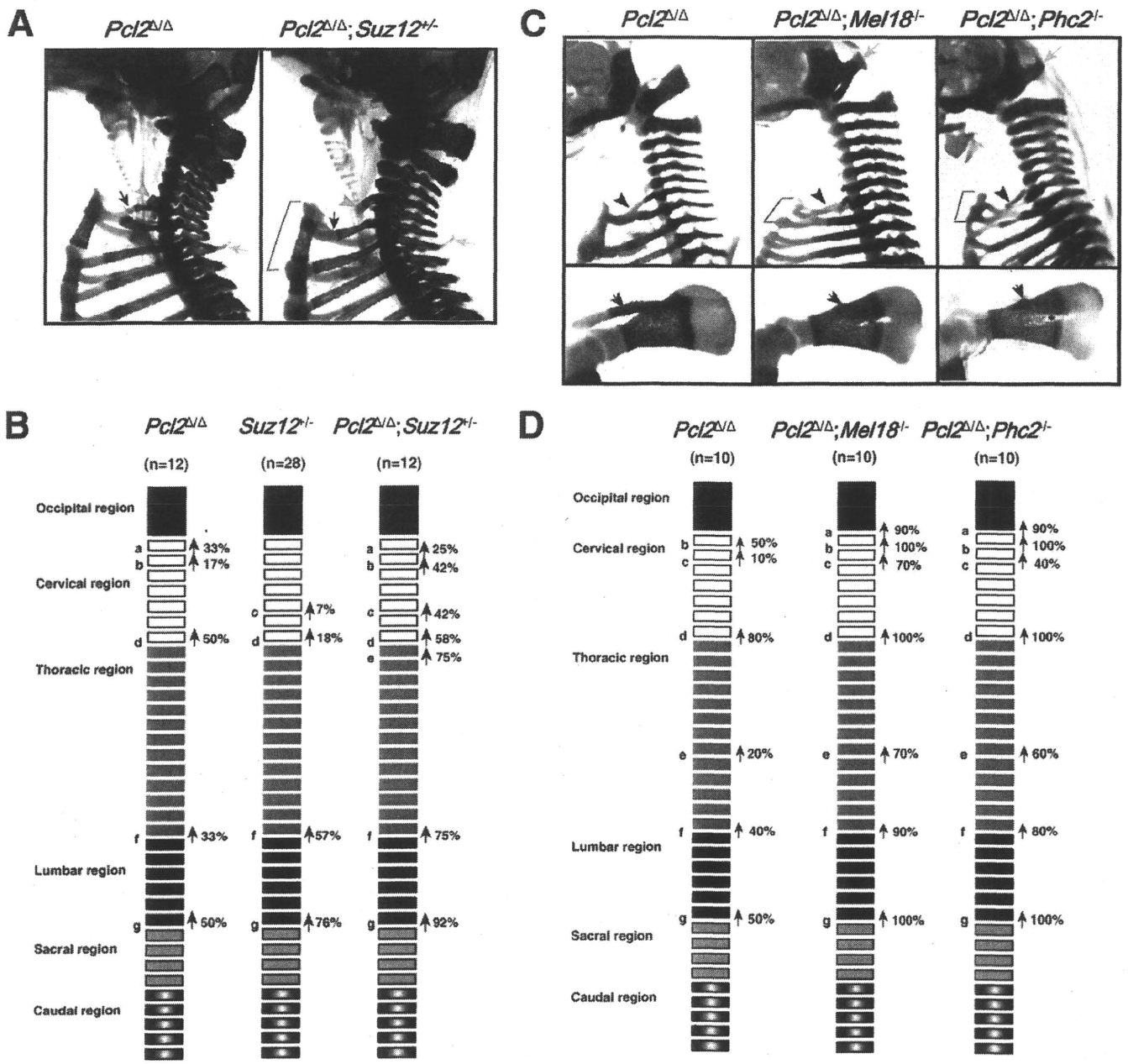

FIG. 5. Synergistic activity of Pcl2 with PRC2 and PRC1 components during A-P specification of the axis. (A) Lateral views of the upper part of the vertebral column in $Pcl2^{\Delta/\Delta}$ and $Pcl2^{\Delta/\Delta}$; $Suz12^{+/-}$ newborn mice. Genotypes of *Pcl2* and *Suz12* loci are indicated at the top. Anterior tubercles, ectopic ribs, and prominent spinous processes are indicated by yellow arrowheads, black arrows, and yellow arrows, respectively. A bracket in $Pcl2^{\Delta/\Delta}$; $Suz12^{+/-}$ indicates the cranially shifted sternum. (B) Schematic representation of the frequency of the axial homeotic transformations in respective mutants. The following parameters, identified by letters on the figure, were scored, and the frequency of each alteration is indicated: C1 → C2, presence of the odontoid process on the C1 vertebra (a); C2 → C3, lack of the odontoid process from the C2 vertebra (b); C5 → C6, appearance of the anterior tubercle of the transverse process on the C5 (c); C7 → T1, appearance of cervical ribs on C7 (d); T1 → T2, prominent spinous process on T1 (e); T13 → L1, loss of the rib on 20th vertebra (f); L5 or L6 → S1, formation of the sacroiliac joint in the 25th or 26th vertebra (g). (C) Skeletal alterations seen in $Pcl2^{\Delta/\Delta}$, $Pcl2^{\Delta/\Delta}$; $Mel18^{-/-}$, and $Pcl2^{\Delta/\Delta}$; $Phc2^{-/-}$ mice. Only the mutant *Pcl2*, *Mel18*, and *Phc2* alleles are depicted. (Upper panels show lateral views of the upper part of the vertebral column. Arrowheads indicate ectopic ribs associated with C7. For $Pcl2^{\Delta/\Delta}$; $Mel18^{-/-}$ and $Pcl2^{\Delta/\Delta}$; $Phc2^{-/-}$ mice, yellow arrows and brackets indicate ectopic arches of the occipital bone and cranially shifted sternum, respectively. Lower panels show overviews of the scapula. Acromion are indicated by arrows, which are rudimentary in the compound mutants. Holes (asterisks) were generated in the center of blades in $Pcl2^{\Delta/\Delta}$; $Mel18^{-/-}$ and $Pcl2^{\Delta/\Delta}$; $Phc2^{-/-}$ mice. (D) Schematic representation of the frequency of the axial homeotic transformations in respective mutants. The following parameters, identified by letters on the figure, were scored, and the frequency of each alteration is indicated: supraoccipital bone → C1, appearance of ectopic bones seen in the craniodorsal region of the C1 vertebra or ectopic arch of the occipital bones (a); C1 → C2, presence of the odontoid process on the C1 vertebra (b); C2 → C3, lack of the odontoid process from the C2 vertebra (c); C7 → T1, appearance of cervical ribs on C7 (d); T7 → T8, dissociation of seventh rib from the sternum (e); T13 → L1, loss of the rib on the 20th vertebra (f); L5 or L6 → S1, formation of the sacroiliac joint in 25th or 26th vertebra (g).

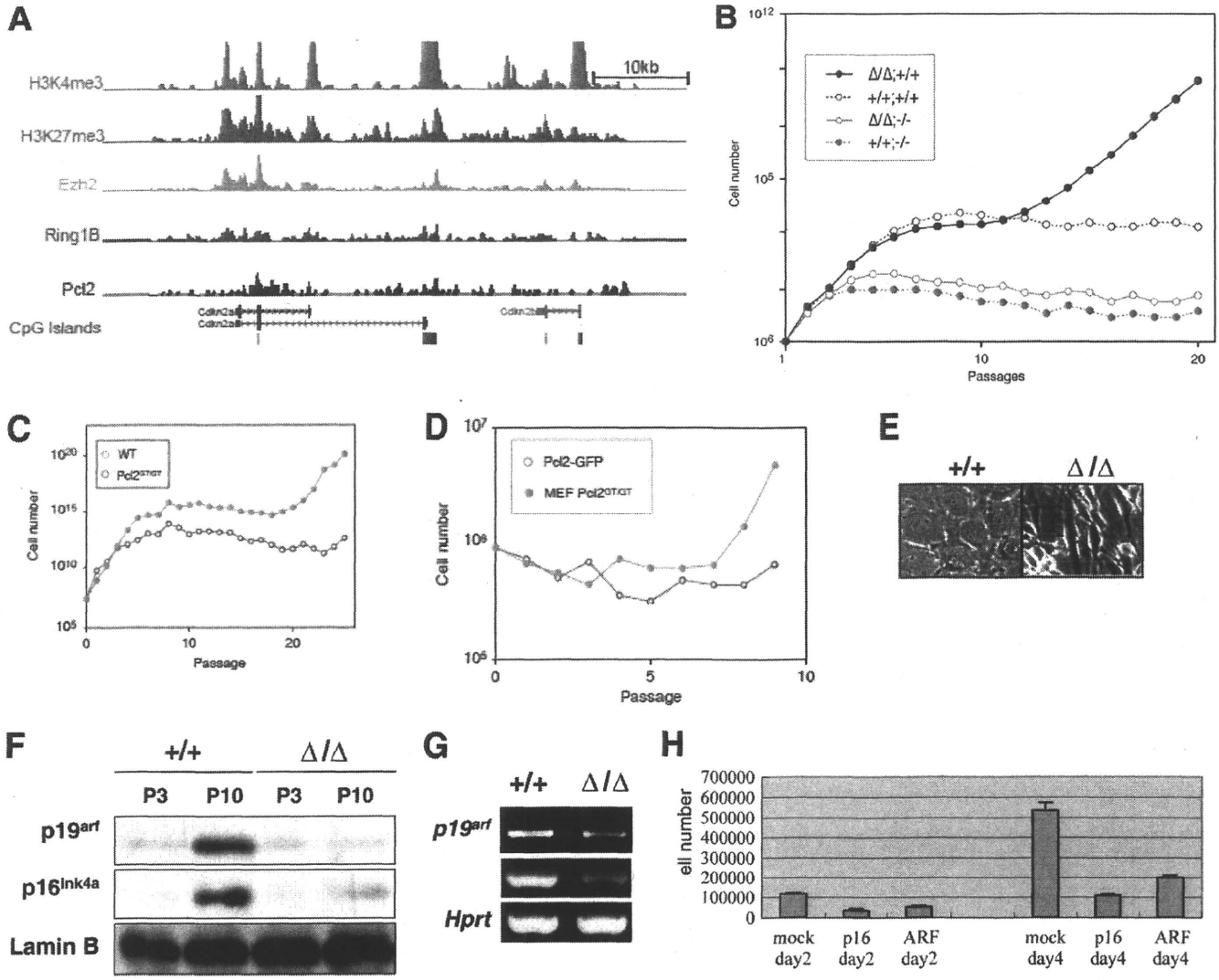

FIG. 6. The role of Pcl2 in replicative senescence. (A) ChIP-seq binding patterns at *Cdkn2a* and *Cdkn2b* loci are shown for H3K4me3, H3K27me3, Ezh2, Ring1B, and Pcl2 in ES cells. CpG islands are shown as green bars (below) (B) Termination of replicative senescence in $Pcl2^{\Delta/\Delta}$ MEFs as revealed by a modified 3T9 assay. Levels of replicative senescence were compared among the wild-type (+/+; +/+), $Pcl2^{\Delta/\Delta}$ (Δ/Δ; +/+), $Phc2^{-/-}$ (+/+; −/−) and $Pcl2^{\Delta/\Delta}$; $Phc2^{-/-}$ (Δ/Δ; −/−) cells. (C) The role of Pcl2 in replicative senescence. Termination of replicative senescence in $Pcl2^{GT/GT}$ MEFs as revealed by a modified 3T9 assay. Levels of replicative senescence were compared between the wild-type (+/+; +/+) and $Pcl2^{GT/GT}$ MEFs. (D) Overexpression of Pcl2 induced senescence in $Pcl2^{GT/GT}$ MEFs. (E) Morphology of wild-type (+/+) and $Pcl2^{\Delta/\Delta}$ (Δ/Δ) MEFs at passage 12. Light microscopic views are shown. (F) Decreased expression of $p19^{arf}$ and $p16^{ink4a}$ in $Pcl2^{\Delta/\Delta}$ (Δ/Δ) MEFs at passage 10 in comparison with that of the wild type (+/+). The expression of lamin B was examined as a dose control. (G) Quantitative analysis of $p19^{arf}$ and $p16^{ink4a}$ transcripts in $Pcl2^{\Delta/\Delta}$ (Δ/Δ) MEFs at passage 10. Note the concomitant reduction of these transcripts in $Pcl2^{\Delta/\Delta}$ MEFs in comparison with wild type (+/+). (H) *Cdkn2a* repression is involved in inhibiting cellular senescence in $Pcl2^{\Delta/\Delta}$ MEFs. Overexpression of either $p19^{arf}$ or $p16^{Ink4a}$ in $Pcl2^{\Delta/\Delta}$ MEFs considerably inhibited their proliferation. The total cells were counted on day 2 and day 4 after retroviral transduction.

stopped replicating at passage 5. Therefore, the *Pcl2*-deficient phenotype was strongly suppressed by loss of *Phc2*, which implies that Pcl2 functions require PRC1 in regulation of cellular senescence. Consistently, we found a considerable quantity of Ring1B retained at the $p16^{Ink4a}$ promoter in $Pcl2^{GT/GT}$ MEFs although its local level was significantly decreased compared to that of the wild type (Fig. 8A and B). Pcl2 thus profoundly modulates functional engagement of PRC2 and PRC1 to maintain proper expression of *Cdkn2a* under replicative stress.

DISCUSSION

In this study, we have investigated the role of Pcl2 at two canonical Polycomb targets, the *Hox* cluster and *Cdkn2a* genes, by combining genetic and biochemical approaches. We have first identified Pcl2 gene products and their functions in *Hox* repression during A-P specification by using two mutant alleles. The expression of Pcl2 and its binding to *Hox* genes were shown to depend on its physical association with PRC2. Interactions of mutant *Pcl2* with *Suz12* indicated the requirement of

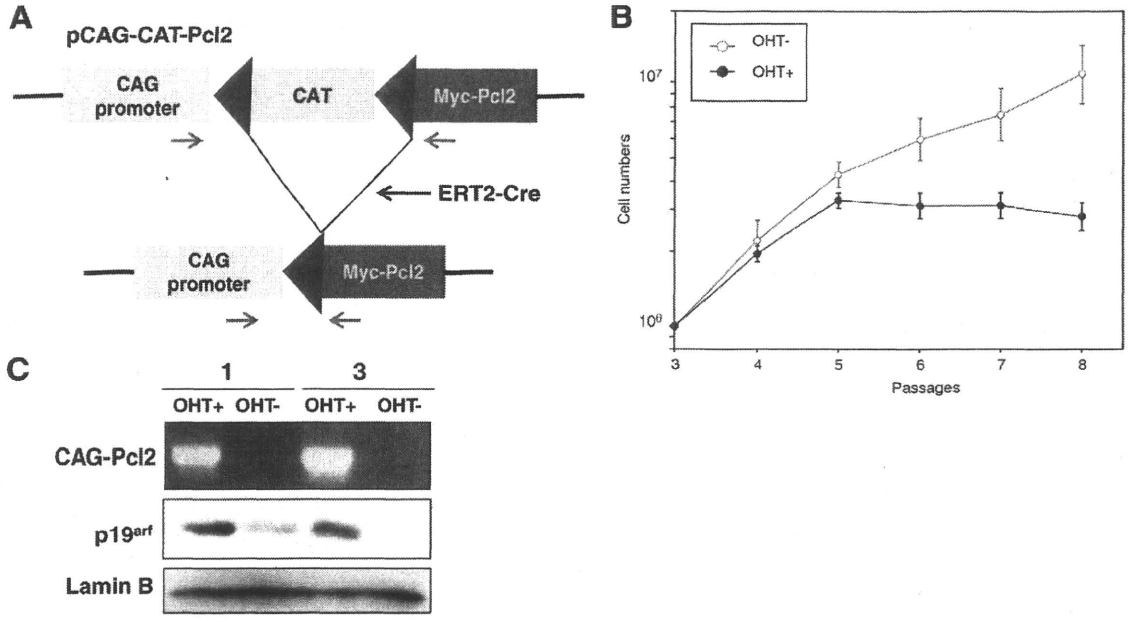

FIG. 7. Pcl2 regulates cellular senescence through *Cdkn2a*. (A) Schematic representation of the transgene to overexpress Myc-tagged Pcl2 in a Cre recombinase-dependent manner. Briefly, the *lacZ* gene in CAG-CAT-Z (4) was replaced by Myc-tagged Pcl2. Pcl2 expression is therefore induced by deletion of chloramphenicol acetyltransferase (CAT) gene cassette placed between two *loxP* sites (shown by arrows) by Cre recombinase. A transgenic line harboring this inducible construct was bred with another transgenic line expressing ERT2-Cre to generate MEFs in which Pcl2 could be expressed upon 4-hydroxytamoxifen ([OHT] 0.5 μM) treatment. The location of primers used to assess deletion of the CAT gene cassette is shown. (B) Impact of Myc-tagged Pcl2 on replicative senescence as revealed by a modified 3T9 assay. Double transgenic MEFs were treated by 0.5 μM tamoxifen at passage 3 (OHT+), and growth rate was examined after the treatment by using untreated MEFs as a control (OHT−). Overexpression of Pcl2 (OHT+) clearly induced premature proliferation arrest. (C) Induction of $p19^{arf}$ expression upon deletion of the CAT gene in two different MEF lines harboring double transgenes. The top panel is an assessment of tamoxifen-induced recombination of the transgene, the middle shows results of Western blotting for $p19^{arf}$ expression, and the bottom shows results of Western blotting for lamin B expression as dose controls.

Pcl2 for PRC2 to exert its functions in *Hox* repression. Therefore, Pcl2 is a functional component of PRC2. It is also noteworthy, however, that the *Pcl2* mutation affects PRC1-mediated repression of *Hox* genes as manifested by genetic interactions between *Pcl2* and *Mel18* or *Phc2* although local depositions of H3K27me3 or Ring1B were not significantly altered in the *Pcl2* mutants. Although the detailed underlying mechanisms are as yet unclear, our results strongly indicate that Pcl2 cooperates with both PRC2 and PRC1 to regulate the expression of *Hox* cluster genes during axial development (Fig. 8C). In contrast, Pcl2 activates the expression of *Cdkn2a* genes once primary fibroblasts become predisposed to stress-induced senescence (Fig. 8C). In this case, Pcl2 could primarily act by suppressing the local catalytic activity of PRC2, which may in turn enable bypassing of PRC1-mediated repression. Taken together, these results show that Pcl2 is required to modify the functional engagement of PRC2 and PRC1 complexes, presumably by sensing cellular circumstances. However, we could not unequivocally exclude the possibility that Pcl2 might have functions independent of PRC2 in regulation of cellular senescence.

Molecular mechanisms that link Pcl2 to such cellular circumstances remain as yet unknown. One intriguing possibility is that Pcl2 might recognize local chromatin cues by its Tudor domain and/or PHD fingers. By using the $Pcl2^{\Delta}$ allele, we have shown a requirement for the 67- and 55-kDa isoforms of Pcl2 to mediate *Hox* repression in developing embryos and *Cdkn2a* activation in MEFs. Based on other recent studies, both Tudor and PHD finger domains have emerged as binding modules for methylated histone tails (7, 26, 34). Particularly, the PHD fingers of Pcl2 are predicted to recognize unmethylated or trimethylated histone H3K4 based on their respective primary structures (42, 52, 60, 65). Polycomb target genes, including *Hox* genes, are known to be bivalently marked by H3K27me3 and H3K4me3 in several cell types. Pcl2 may contribute to the *Hox* regulation via its recognition of the methylation status of H3K4 in developing embryos. In addition to detection of the methylation status of histone tails, Tudor and PHD finger domains have also been shown to contribute to recognition of RNA and phosphatidylinositols, respectively (7, 22, 26). We thus postulate that Pcl2 might use a combination of the Tudor domain and PHD fingers to discern chromatin circumstances and affect local activity of PRC2 via physical interaction. Identification of ligands for the Pcl2 Tudor domain and PHD fingers will be necessary to fully clarify this issue.

It is well known that the expression of *Hox* genes continues to be dynamically regulated in developing tissues after the initial establishment of their early expression domains (16). This implies that Polycomb-dependent *Hox* repression is plastic with the potential to be reactivated, presumably by various differentiation cues. In line with this, PRC1 has been shown to be linked to inductive signals mediating cellular differentiation, survival, and/or proliferation in cerebellar progenitors and ES cells (18, 39). Moreover, recent studies demonstrate that dy-

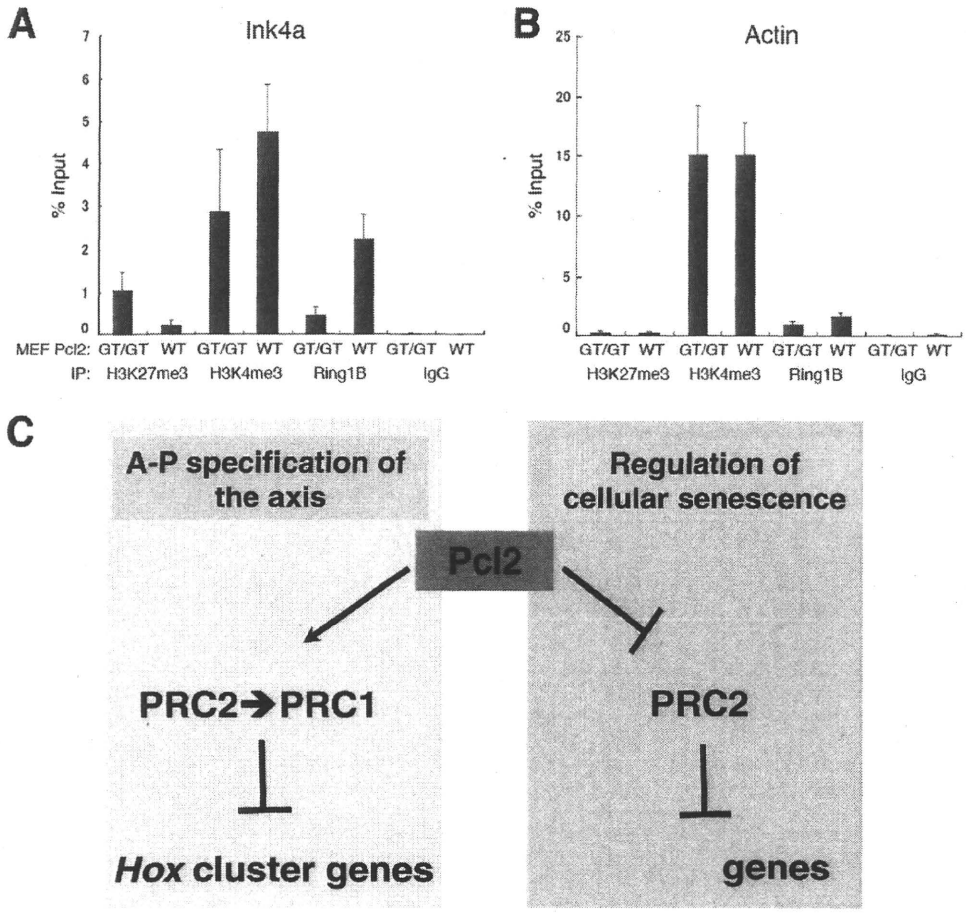

FIG. 8. The role of Pcl2 for PRC2 and PRC1. (A and B) Enrichment of H3K27me3, H3K4me3, and Ring1B at the $p16^{Ink4a}$ promoter region was determined by ChIP and site-specific real-time PCR. The β-actin promoter was used as a control. (C) A model for Pcl2 functions during A-P specification of the axis and stress-induced cellular senescence. In developing embryos, Pcl2 is a functional component of PRC2 and also functionally cooperates with PRC1 to mediate repression of *Hox* cluster genes. Upon replicative stress, Pcl2 activates *Cdkn2a* expression and suppresses cellular senescence, likely by suppressing the catalytic activity of PRC2 at the *Cdkn2a* locus.

namic regulation of Polycomb activity orchestrated by the Jumonji (or Jarid2) protein included in PRC2 balances self-renewal and differentiation of ES cells (58). In this regard, it is worthy of note that Pcl2 is copurified with Jumonji (41). Pcl2, in collaboration with proteins such as Jumonji, could act as a module that mediates such plasticity of Polycomb repression by discerning chromatin circumstances induced by differentiation cues.

ACKNOWLEDGMENT

This project was in part supported by Genome Network Project from the Ministry of Education, Culture, Sports, Science and Technology of the Japanese Government (H.K.).

REFERENCES

1. **Akasaka, T., M. Kanno, R. Balling, M. A. Mieza, M. Taniguchi, and H. Koseki.** 1996. A role for mel-18, a Polycomb group-related vertebrate gene, during the anteroposterior specification of the axial skeleton. Development **122:**1513–1522.
2. **Akasaka, T., M. van Lohuizen, N. van der Lugt, Y. Mizutani-Koseki, M. Kanno, M. Taniguchi, M. Vidal, M. Alkema, A. Berns, and H. Koseki.** 2001. Mice doubly deficient for the Polycomb group genes Mel18 and Bmi1 reveal synergy and requirement for maintenance but not initiation of Hox gene expression. Development **128:**1587–1597.
3. **Altschul, S. F., W. Gish, W. Miller, E. W. Myers, and D. J. Lipman.** 1990. Basic local alignment search tool. J. Mol. Biol. **215:**403–410.
4. **Araki, K., M. Araki, J. Miyazaki, and P. Vassalli.** 1995. Site-specific recombination of a transgene in fertilized eggs by transient expression of Cre recombinase. Proc. Natl. Acad. Sci. U. S. A. **92:**160–164.
5. **Atsuta, T., S. Fujimura, H. Moriya, M. Vidal, T. Akasaka, and H. Koseki.** 2001. Production of monoclonal antibodies against mammalian Ring1B proteins. Hybridoma **20:**43–46.
6. **Bel, S., N. Core, M. Djabali, K. Kieboom, N. Van der Lugt, M. J. Alkema, and M. Van Lohuizen.** 1998. Genetic interactions and dosage effects of Polycomb group genes in mice. Development **125:**3543–3551.
7. **Bernstein, E., and C. D. Allis.** 2005. RNA meets chromatin. Genes Dev. **19:**1635–1655.
8. **Boyer, L. A., K. Plath, J. Zeitlinger, T. Brambrink, L. A. Medeiros, T. I. Lee, S. S. Levine, M. Wernig, A. Tajonar, M. K. Ray, G. W. Bell, A. P. Otte, M. Vidal, D. K. Gifford, R. A. Young, and R. Jaenisch.** 2006. Polycomb complexes repress developmental regulators in murine embryonic stem cells. Nature **441:**349–353.
9. **Cao, R., Y. Tsukada, and Y. Zhang.** 2005. Role of Bmi-1 and Ring1A in H2A ubiquitylation and Hox gene silencing. Mol. Cell **20:**845–854.
10. **Cao, R., H. Wang, J. He, H. Erdjument-Bromage, P. Tempst, and Y. Zhang.** 2008. Role of hPHF1 in H3K27 methylation and Hox gene silencing. Mol. Cell. Biol. **28:**1862–1872.
11. **Cao, R., L. Wang, H. Wang, L. Xia, H. Erdjument-Bromage, P. Tempst, R. S. Jones, and Y. Zhang.** 2002. Role of histone H3 lysine 27 methylation in Polycomb-group silencing. Science **298:**1039–1043.
12. **Coulson, M., S. Robert, H. J. Eyre, and R. Saint.** 1998. The identification and localization of a human gene with sequence similarity to Polycomblike of *Drosophila melanogaster*. Genomics **48:**381–383.
13. **Czermin, B., R. Melfi, D. McCabe, V. Seitz, A. Imhof, and V. Pirrotta.** 2002. *Drosophila* enhancer of Zeste/ESC complexes have a histone H3 methyl-

transferase activity that marks chromosomal Polycomb sites. Cell **111:**185–196.
14. **de Napoles, M., J. E. Mermoud, R. Wakao, Y. A. Tang, M. Endoh, R. Appanah, T. B. Nesterova, J. Silva, A. P. Otte, M. Vidal, H. Koseki, and N. Brockdorff.** 2004. Polycomb group proteins Ring1A/B link ubiquitylation of histone H2A to heritable gene silencing and X inactivation. Dev. Cell **7:**663–676.
15. **Dignam, J. D., R. M. Lebovitz, and R. G. Roeder.** 1983. Accurate transcription initiation by RNA polymerase II in a soluble extract from isolated mammalian nuclei. Nucleic Acids Res. **11:**1475–1489.
16. **Duboule, D.** 1995. Vertebrate Hox genes and proliferation: an alternative pathway to homeosis? Curr. Opin. Genet. Dev. **5:**525–528.
17. **Duncan, I. M.** 1982. Polycomblike: a gene that appears to be required for the normal expression of the bithorax and antennapedia gene complexes of *Drosophila melanogaster*. Genetics **102:**49–70.
18. **Endoh, M., T. A. Endo, T. Endoh, Y. Fujimura, O. Ohara, T. Toyoda, A. P. Otte, M. Okano, N. Brockdorff, M. Vidal, and H. Koseki.** 2008. Polycomb group proteins Ring1A/B are functionally linked to the core transcriptional regulatory circuitry to maintain ES cell identity. Development **135:**1513–1524.
19. **Eskeland, R., M. Leeb, G. R. Grimes, C. Kress, S. Boyle, D. Sproul, N. Gilbert, Y. Fan, A. I. Skoultchi, A. Wutz, and W. A. Bickmore.** 2010. Ring1B compacts chromatin structure and represses gene expression independent of histone ubiquitination. Mol. Cell **38:**452–464.
20. **Francis, N. J., A. J. Saurin, Z. Shao, and R. E. Kingston.** 2001. Reconstitution of a functional core polycomb repressive complex. Mol. Cell **8:**545–556.
21. **Fujimura, Y., K. Isono, M. Vidal, M. Endoh, H. Kajita, Y. Mizutani-Koseki, Y. Takihara, M. van Lohuizen, A. Otte, T. Jenuwein, J. Deschamps, and H. Koseki.** 2006. Distinct roles of Polycomb group gene products in transcriptionally repressed and active domains of Hoxb8. Development **133:**2371–2381.
22. **Gozani, O., P. Karuman, D. R. Jones, D. Ivanov, J. Cha, A. A. Lugovskoy, C. L. Baird, H. Zhu, S. J. Field, S. L. Lessnick, J. Villasenor, B. Mehrotra, J. Chen, V. R. Rao, J. S. Brugge, C. G. Ferguson, B. Payrastre, D. G. Myszka, L. C. Cantley, G. Wagner, N. Divecha, G. D. Prestwich, and J. Yuan.** 2003. The PHD finger of the chromatin-associated protein ING2 functions as a nuclear phosphoinositide receptor. Cell **114:**99–111.
23. **Hamer, K. M., R. G. Sewalt, J. L. den Blaauwen, T. Hendrix, D. P. Satijn, and A. P. Otte.** 2002. A panel of monoclonal antibodies against human polycomb group proteins. Hybrid. Hybridomics **21:**245–252.
24. **Hansen, J., T. Floss, P. Van Sloun, E. M. Fuchtbauer, F. Vauti, H. H. Arnold, F. Schnutgen, W. Wurst, H. von Melchner, and P. Ruiz.** 2003. A large-scale, gene-driven mutagenesis approach for the functional analysis of the mouse genome. Proc. Natl. Acad. Sci. U. S. A. **100:**9918–9922.
25. **Hong, Z., J. Jiang, L. Lan, S. Nakajima, S. Kanno, H. Koseki, and A. Yasui.** 2008. A polycomb group protein, PHF1, is involved in the response to DNA double-strand breaks in human cell. Nucleic Acids Res. **36:**2939–2947.
26. **Huyen, Y., O. Zgheib, R. A. Ditullio, Jr., V. G. Gorgoulis, P. Zacharatos, T. J. Petty, E. A. Sheston, H. S. Mellert, E. S. Stavridi, and T. D. Halazonetis.** 2004. Methylated lysine 79 of histone H3 targets 53BP1 to DNA double-strand breaks. Nature **432:**406–411.
27. **Inouye, C., P. Remondelli, M. Karin, and S. Elledge.** 1994. Isolation of a cDNA encoding a metal response element binding protein using a novel expression cloning procedure: the one hybrid system. DNA Cell Biol. **13:**731–742.
28. **Isono, K., Y. Fujimura, J. Shinga, M. Yamaki, J. O. Wang, Y. Takihara, Y. Murahashi, Y. Takada, Y. Mizutani-Koseki, and H. Koseki.** 2005. Mammalian polyhomeotic homologues Phc2 and Phc1 act in synergy to mediate polycomb repression of *Hox* genes. Mol. Cell. Biol. **25:**6694–6706.
29. **Isono, K., Y. Mizutani-Koseki, T. Komori, M. S. Schmidt-Zachmann, and H. Koseki.** 2005. Mammalian polycomb-mediated repression of Hox genes requires the essential spliceosomal protein Sf3b1. Genes Dev. **19:**536–541.
30. **Jacobs, J. J., K. Kieboom, S. Marino, R. A. DePinho, and M. van Lohuizen.** 1999. The oncogene and Polycomb-group gene *bmi-1* regulates cell proliferation and senescence through the *ink4a* locus. Nature **397:**164–168.
31. **Kamijo, T., F. Zindy, M. F. Roussel, D. E. Quelle, J. R. Downing, R. A. Ashmun, G. Grosveld, and C. J. Sherr.** 1997. Tumor suppression at the mouse INK4a locus mediated by the alternative reading frame product p19ARF. Cell **91:**649–659.
32. **Kawakami, S., K. Mitsunaga, Y. Y. Kikuti, A. Ando, H. Inoko, K. Yamamura, and K. Abe.** 1998. Tctex3, related to *Drosophila* polycomblike, is expressed in male germ cells and mapped to the mouse t-complex. Mamm. Genome **9:**874–880.
33. **Kennison, J. A., and J. W. Tamkun.** 1988. Dosage-dependent modifiers of polycomb and antennapedia mutations in *Drosophila*. Proc. Natl. Acad. Sci. U. S. A. **85:**8136–8140.
34. **Kim, J., J. Daniel, A. Espejo, A. Lake, M. Krishna, L. Xia, Y. Zhang, and M. T. Bedford.** 2006. Tudor, MBT and chromo domains gauge the degree of lysine methylation. EMBO Rep. **7:**397–403.
35. **King, I. F., N. J. Francis, and R. E. Kingston.** 2002. Native and recombinant Polycomb group complexes establish a selective block to template accessibility to repress transcription in vitro. Mol. Cell. Biol. **22:**7919–7928.
36. **Kitaguchi, T., K. Nakata, T. Nagai, J. Aruga, and K. Mikoshiba.** 2001. *Xenopus* Polycomblike 2 (XPcl2) controls anterior to posterior patterning of the neural tissue. Dev. Genes Evol. **211:**309–314.
37. **Ku, M., R. P. Koche, E. Rheinbay, E. M. Mendenhall, M. Endoh, T. S. Mikkelsen, A. Presser, C. Nusbaum, X. Xie, A. S. Chi, M. Adli, S. Kasif, L. M. Ptaszek, C. A. Cowan, E. S. Lander, H. Koseki, and B. E. Bernstein.** 2008. Genomewide analysis of PRC1 and PRC2 occupancy identifies two classes of bivalent domains. PLoS Genet. **4:**e1000242.
38. **Lee, T. I., R. G. Jenner, L. A. Boyer, M. G. Guenther, S. S. Levine, R. M. Kumar, B. Chevalier, S. E. Johnstone, M. F. Cole, K. Isono, H. Koseki, T. Fuchikami, K. Abe, H. L. Murray, J. P. Zucker, B. Yuan, G. W. Bell, E. Herbolsheimer, N. M. Hannett, K. Sun, D. T. Odom, A. P. Otte, T. L. Volkert, D. P. Bartel, D. A. Melton, D. K. Gifford, R. Jaenisch, and R. A. Young.** 2006. Control of developmental regulators by Polycomb in human embryonic stem cells. Cell **125:**301–313.
39. **Leung, C., M. Lingbeek, O. Shakhova, J. Liu, E. Tanger, P. Saremaslani, M. Van Lohuizen, and S. Marino.** 2004. Bmi1 is essential for cerebellar development and is overexpressed in human medulloblastomas. Nature **428:**337–341.
40. **Levine, S. S., A. Weiss, H. Erdjument-Bromage, Z. Shao, P. Tempst, and R. E. Kingston.** 2002. The core of the Polycomb repressive complex is compositionally and functionally conserved in flies and humans. Mol. Cell. Biol. **22:**6070–6078.
41. **Li, G., R. Margueron, M. Ku, P. Chambon, B. E. Bernstein, and D. Reinberg.** 2010. Jarid2 and PRC2, partners in regulating gene expression. Genes Dev. **24:**368–380.
42. **Li, H., S. Ilin, W. Wang, E. M. Duncan, J. Wysocka, C. D. Allis, and D. J. Patel.** 2006. Molecular basis for site-specific read-out of histone H3K4me3 by the BPTF PHD finger of NURF. Nature **442:**91–95.
43. **Lonie, A., R. D'Andrea, R. Paro, and R. Saint.** 1994. Molecular characterisation of the Polycomblike gene of *Drosophila melanogaster*, a trans-acting negative regulator of homeotic gene expression. Development **120:**2629–2636.
44. **Mikkelsen, T. S., M. Ku, D. B. Jaffe, B. Issac, E. Lieberman, G. Giannoukos, P. Alvarez, W. Brockman, T. K. Kim, R. P. Koche, W. Lee, E. Mendenhall, A. O'Donovan, A. Presser, C. Russ, X. Xie, A. Meissner, M. Wernig, R. Jaenisch, C. Nusbaum, E. S. Lander, and B. E. Bernstein.** 2007. Genome-wide maps of chromatin state in pluripotent and lineage-committed cells. Nature **448:**553–560.
45. **Mortazavi, A., B. A. Williams, K. McCue, L. Schaeffer, and B. Wold.** 2008. Mapping and quantifying mammalian transcriptomes by RNA-Seq. Nat. Methods **5:**621–628.
46. **Muller, J., C. M. Hart, N. J. Francis, M. L. Vargas, A. Sengupta, B. Wild, E. L. Miller, M. B. O'Connor, R. E. Kingston, and J. A. Simon.** 2002. Histone methyltransferase activity of a *Drosophila* Polycomb group repressor complex. Cell **111:**197–208.
47. **Nekrasov, M., T. Klymenko, S. Fraterman, B. Papp, K. Oktaba, T. Kocher, A. Cohen, H. G. Stunnenberg, M. Wilm, and J. Muller.** 2007. Pcl-PRC2 is needed to generate high levels of H3-K27 trimethylation at Polycomb target genes. EMBO J. **26:**4078–4088.
48. **O'Carroll, D., S. Erhardt, M. Pagani, S. C. Barton, M. A. Surani, and T. Jenuwein.** 2001. The *Polycomb*-group gene *Ezh2* is required for early mouse development. Mol. Cell. Biol. **21:**4330–4336.
49. **O'Connell, S., L. Wang, S. Robert, C. A. Jones, R. Saint, and R. S. Jones.** 2001. Polycomblike PHD fingers mediate conserved interaction with enhancer of zeste protein. J. Biol. Chem. **276:**43065–43073.
50. **Paro, R.** 1995. Propagating memory of transcriptional states. Trends Genet. **11:**295–297.
51. **Pasini, D., A. P. Bracken, M. R. Jensen, E. Lazzerini Denchi, and K. Helin.** 2004. Suz12 is essential for mouse development and for EZH2 histone methyltransferase activity. EMBO J. **23:**4061–4071.
52. **Pena, P. V., F. Davrazou, X. Shi, K. L. Walter, V. V. Verkhusha, O. Gozani, R. Zhao, and T. G. Kutateladze.** 2006. Molecular mechanism of histone H3K4me3 recognition by plant homeodomain of ING2. Nature **442:**100–103.
53. **Pirrotta, V.** 1997. PcG complexes and chromatin silencing. Curr. Opin. Genet. Dev. **7:**249–258.
54. **Sakai, K., and J. Miyazaki.** 1997. A transgenic mouse line that retains Cre recombinase activity in mature oocytes irrespective of the *cre* transgene transmission. Biochem. Biophys. Res. Commun. **237:**318–324.
55. **Sarma, K., R. Margueron, A. Ivanov, V. Pirrotta, and D. Reinberg.** 2008. Ezh2 requires PHF1 to efficiently catalyze H3 lysine 27 trimethylation in vivo. Mol. Cell. Biol. **28:**2718–2731.
56. **Savla, U., J. Benes, J. Zhang, and R. S. Jones.** 2008. Recruitment of *Drosophila* Polycomb-group proteins by Polycomblike, a component of a novel protein complex in larvae. Development **135:**813–817.
57. **Shao, Z., F. Raible, R. Mollaaghababa, J. R. Guyon, C. T. Wu, W. Bender, and R. E. Kingston.** 1999. Stabilization of chromatin structure by PRC1, a Polycomb complex. Cell **98:**37–46.
58. **Shen, X., W. Kim, Y. Fujiwara, M. D. Simon, Y. Liu, M. R. Mysliwiec, G. C. Yuan, Y. Lee, and S. H. Orkin.** 2009. Jumonji modulates polycomb activity and self-renewal versus differentiation of stem cells. Cell **139:**1303–1314.

59. **Sherr, C. J., and R. A. DePinho.** 2000. Cellular senescence: mitotic clock or culture shock? Cell **102**:407–410.
60. **Shi, X., T. Hong, K. L. Walter, M. Ewalt, E. Michishita, T. Hung, D. Carney, P. Pena, F. Lan, M. R. Kaadige, N. Lacoste, C. Cayrou, F. Davrazou, A. Saha, B. R. Cairns, D. E. Ayer, T. G. Kutateladze, Y. Shi, J. Cote, K. F. Chua, and O. Gozani.** 2006. ING2 PHD domain links histone H3 lysine 4 methylation to active gene repression. Nature **442**:96–99.
61. **Shumacher, A., C. Faust, and T. Magnuson.** 1996. Positional cloning of a global regulator of anterior-posterior patterning in mice. Nature **383**:250–253.
62. **Tie, F., J. Prasad-Sinha, A. Birve, A. Rasmuson-Lestander, and P. J. Harte.** 2003. A 1-megadalton ESC/E(Z) complex from *Drosophila* that contains polycomblike and RPD3. Mol. Cell. Biol. **23**:3352–3362.
63. **Walker, E., W. Y. Chang, J. Hunkapiller, G. Cagney, K. Garcha, J. Torchia, N. J. Krogan, J. F. Reiter, and W. L. Stanford.** 2010. Polycomb-like 2 associates with PRC2 and regulates transcriptional networks during mouse embryonic stem cell self-renewal and differentiation. Cell Stem Cell **6**:153–166.
64. **Wang, H., L. Wang, H. Erdjument-Bromage, M. Vidal, P. Tempst, R. S. Jones, and Y. Zhang.** 2004. Role of histone H2A ubiquitination in Polycomb silencing. Nature **431**:873–878.
65. **Wang, S., F. He, W. Xiong, S. Gu, H. Liu, T. Zhang, X. Yu, and Y. Chen.** 2007. Polycomblike-2-deficient mice exhibit normal left-right asymmetry. Dev. Dyn. **236**:853–861.
66. **Wang, S., X. Yu, T. Zhang, X. Zhang, Z. Zhang, and Y. Chen.** 2004. Chick Pcl2 regulates the left-right asymmetry by repressing Shh expression in Hensen's node. Development **131**:4381–4391.